SYNCHRONIZATION OF SOQPSK-TG IN BURST-MODE TRANSMISSIONS

Ehsan Hosseini
Department of Electrical Engineering & Computer Science
University of Kansas
Lawrence, KS 66045
ehsan@ku.edu

Faculty Advisor:
Erik Perrins

ABSTRACT

In this paper, we present a maximum likelihood synchronization algorithm which jointly estimates frequency offset, symbol timing and carrier phase for shaped-offset quadrature phase-shift keying (SOQPSK) signals. We have considered a burst-mode transmission scenario in which a known training sequence is embedded in the beginning of each burst for the purpose of data-aided (DA) synchronization in a feedforward structure. The proposed algorithm first estimates the frequency offset independently from other parameters. The estimated frequency is then used to derive the symbol timing which is followed by the carrier phase estimation. The mean-squared error (MSE) of the proposed algorithm is computed via simulations. The results show that the proposed algorithm performs near the theoretical Cramér-Rao bound (CRB) at signal-to-noise ratios (SNRs) as low as 0 dB.

INTRODUCTION

Shaped-offset quadrature phase shift-keying (SOQPSK) is a physical-layer waveform that has seen extensive use in serial streaming telemetry (SST), and has been selected for future use in the integrated network enhanced telemetry (iNET) system. A key difference between SST and iNET is that iNET uses burst-mode transmission. The synchronization task becomes more challenging in burst-mode transmissions because there is little time for acquiring and locking onto the signal.

In this paper, we introduce a maximum likelihood (ML) algorithm for feedforward DA synchronization of SOQPSK signals when transmitted over an additive-white Gaussian noise (AWGN) channel. Our algorithm jointly estimates the symbol timing, carrier phase and frequency offset based a known training sequence. The proposed approach first estimates the frequency offset from the collected samples corresponding to the training sequence. Once the frequency offset is known, the symbol timing is estimated, which is followed by the carrier phase estimation. The performance of the proposed method is investigated for two well-known SOQPSK schemes via simulations. The computed error variances reveal that our algorithm is capable of operating quite close to the theoretical Cramér-Rao bound (CRB) for all the synchronization parameters.

The paper is organized as follows. The next section introduces the transmission model using SOQPSK signaling. Following that, we propose the ML estimation algorithm, which is derived based on the

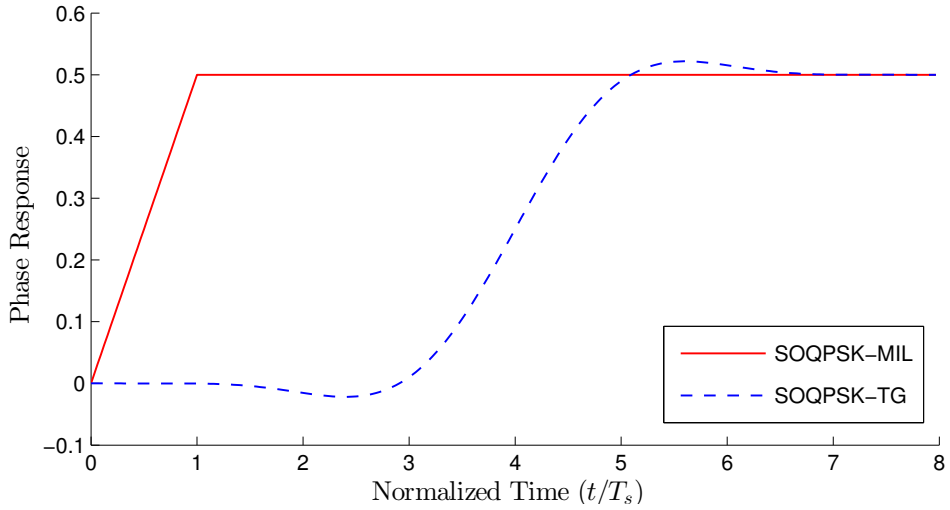

Figure 1: Phase response $q(t)$ for SOQPSK-MIL ($L = 1$) and SOQPSK-TG ($L = 8$).

characteristics of the optimum training sequence. We then explain practical considerations for the implementation of our method. We conclude by illustrating the performance of the proposed algorithm in terms of the frequency, timing and phase error variances for different SOQPSK schemes.

SOQPSK-TG SIGNAL MODEL

In our model, we assume each burst starts with a preamble, which is comprised of L_0 symbols having a duration of $T_0 = L_0 T_s$ seconds where T_s is the symbol duration. It is immediately followed by the payload carrying the information symbols. The complex baseband SOQPSK signal during transmission of the preamble can be expressed as

$$s(t) = \sqrt{\frac{E_s}{T_s}} \exp\{j\phi(t;\boldsymbol{\alpha})\} \tag{1}$$

where is E_s is energy per transmitted symbol. The phase of the signal $\phi(t;\boldsymbol{\alpha})$ is defined as

$$\phi(t;\boldsymbol{\alpha}) = 2\pi h \sum_{i=0}^{L_0-1} \alpha_i q(t - iT_s) \tag{2}$$

where α_i is the transmitted ternary symbol, i.e. $\alpha_i \in \{-1, 0, 1\}$, and $h = 1/2$ is the modulation index. The waveform $q(t)$ is the *phase response* of SOQPSK and in general is represented as the integral of the *frequency pulse* $g(t)$ with a duration of LT_s. There are currently two different versions of SOQPSK defined by their own frequency pulses. The first one known as the SOQPSK-MIL [1] is a full-response ($L = 1$) scheme with a rectangular-shaped frequency pulse. The second form is the telemetry group version [2], i.e. SOQPSK-TG, which is partial-response ($L = 8$) with a custom frequency pulse. According to the CPM definition, $q(t)$ is zero for $t < 0$ and is $1/2$ for $t > LT_s$. The phase responses of the aforementioned SOQPSKs are illustrated in Fig. 1.

The SOQPSK modulator can be characterized as a precoder connected to a CPM modulator. The precoder converts information bits $a_i \in \{0, 1\}$ to ternary symbols by means of

$$\alpha_i = (-1)^{i+1}(2a_{i-1} - 1)(a_i - a_{i-2}) \tag{3}$$

in order to impose OQPSK-like characteristics on the CPM signal. In the following, we will perform our analysis based on $\{\alpha_i\}$ because the preamble is fixed and known in terms of the ternary symbols. Note that the precoder does not change the rate of input bits, and hence, $T_b = T_s$.

Assuming transmission over an AWGN channel, the complex baseband representation of the received signal is

$$r(t) = \sqrt{\frac{E_s}{T_s}} e^{j(2\pi f_d t + \theta)} e^{j\phi(t-\tau;\boldsymbol{\alpha})} + w(t) \tag{4}$$

where θ is the unknown carrier phase, f_d is the frequency offset, τ is the timing offset, and $w(t)$ is complex baseband AWGN with zero mean and power spectral density N_0. The transmitted data symbols are denoted by $\boldsymbol{\alpha} = [\alpha_0, \alpha_1, \cdots, \alpha_{L_0-1}]$. In the following, we denote the synchronization parameters as $\mathbf{u} = [f_d, \theta, \tau]^T$, which is the vector of unknown but deterministic parameters which are to be *jointly* estimated at the receiver. Our known preamble is implicit in the definition of $s(t)$. Finally, it is assumed that the start-of-signal (SOS) is already known at the receiver using signal detection methods. Therefore, the symbol timing offset is limited to $-T_s/2 < \tau < T_s/2$.

The proposed preamble for iNET has a length of $L_0 = 128$. This preamble is periodic and it consists of repeating a sequence of 16 information bits 8 times as follows,

$$\left.\begin{array}{rcl} a_{2k} & = & 1,0,1,0,1,0,1,0 \\ a_{2k+1} & = & 1,0,1,1,0,1,0,0 \end{array}\right\} \text{for } k = 0, \ldots, 7. \tag{5}$$

where $\{a_i\}$ is fed into a precoder in which $a_{-2} = a_{-1} = 0$. This results in a sequence of ternary symbols which is depicted in Fig. 2 for one period of the preamble. We denote this preamble by $\boldsymbol{\alpha}^*$ in the rest of our discussion.

MAXIMUM-LIKELIHOOD ESTIMATION

Reliable detection of SOQPSK signals depends on perfect timing and carrier synchronization, which requires the knowledge of τ, θ and f_d. These synchronization parameters can be estimated via various algorithms. In this work, we apply joint maximum-likelihood (ML) estimation in which the data sequence $\boldsymbol{\alpha}$ is known to the receiver. The joint log-likelihood function (LLF) for synchronization parameters is given in [3] for CPM, which can also be applied to SOQPSK. Thus, the LLF in our problem can be expressed (within a constant factor) as

$$\Lambda(\tilde{f}_d, \tilde{\theta}, \tilde{\tau}) = \mathrm{Re}\left[\int_{\tilde{\tau}}^{T_0+\tilde{\tau}} e^{-j(2\pi \tilde{f}_d t + \tilde{\theta})} r(t) s^*(t - \tilde{\tau}) dt\right] \tag{6}$$

where $\tilde{f}_d$, $\tilde{\theta}$ and $\tilde{\tau}$ are hypothetical (i.e., *trial*) values for frequency offset, carrier phase and symbol timing respectively. According to the ML criterion, we choose the trial values that maximize (6) as the best estimates for the unknown parameters $\mathbf{u}$. We denote the ML estimates as $\hat{\mathbf{u}} = [\hat{f}_d, \hat{\theta}, \hat{\tau}]^T$.

Based on (6), the maximization of the LLF requires at least a two dimensional grid search on $(\tilde{f}_d, \tilde{\tau})$ in general because both of these parameters are embedded in the computation of the above integral. Therefore, we are interested in a method which decouples symbol timing and frequency offset.

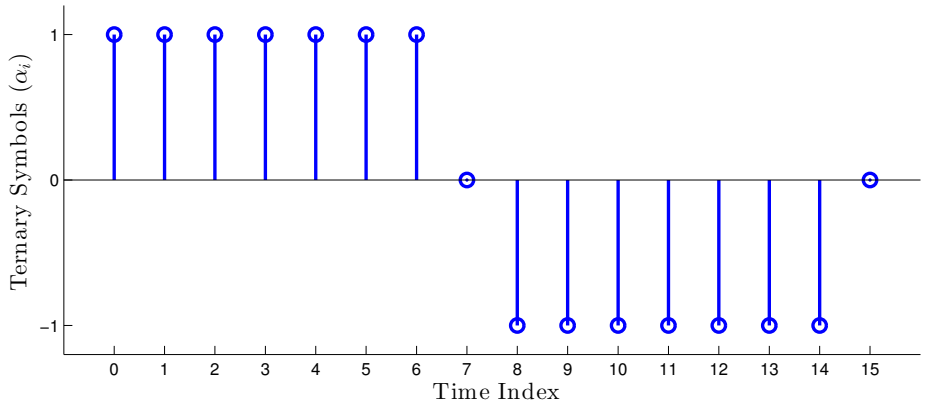

Figure 2: A length-16 period of the ternary symbols in the iNET preamble for SOQPSK-TG. The full length-128 preamble is formed by repeating above sequence 8 times.

Let us investigate $\boldsymbol{\alpha}^*$ and its phase response more carefully. We note that $\boldsymbol{\alpha}^*$, within each period, can be divided into two segments, each of which having the same symbols of either +1 or -1. This pattern causes the SOQPSK phase $\phi(t, \boldsymbol{\alpha})$ to change with a uniform rate of approximately $\pi/2$ radians per symbol in the same direction within each segment. We have illustrated this fact in Fig. 3 by plotting the unwrapped phase response of SOQPSK-MIL and SOQPSK-TG when $\boldsymbol{\alpha}^*$ for its first 32 symbols is utilized. More importantly, SOQPSK-TG's phase response follows a straight line within each part, similar to SOQPSK-MIL, despite its bell-shaped frequency pulse. This is due to the overlapping of its frequency pulses when the subsequent data symbols are the same. This fact leads to a uniform phase variations for SOQPSK-TG. Additionally, the overall phase response is delayed when partial-response SOQPSK-TG is employed. This lag time is depicted by T_l in Fig. 3. Our numerical computations show that the squared error between SOQPSK-TG and SOQPSK-MIL phase responses is minimized when SOQPSK-MIL's response is shifted by $T_l = 3.5T_S$. Finally, it can be observed that the transition points are smoother for SOQPSK-TG because of its partial response behavior, which also makes it more bandwidth-efficient than SOQPSK-MIL.

Based on the above discussion, we approximate the phase response of SOQPSK-TG to $\boldsymbol{\alpha}^*$ with a delayed version of SOQPSK-MIL's response to the same preamble sequence. Its approximated phase response $\phi(t, \boldsymbol{\alpha}^*)$ can be mathematically expressed as

$$\phi(t, \boldsymbol{\alpha}^*) \approx \begin{cases} \frac{\pi(t-16kTs-T_l)}{2T_s} & 16kT_s + T_l < t \leq (16k+8)T_s + T_l \\ -\frac{\pi(t-(16k+15)T_s-T_l)}{2T_s} & (16k+8)T_s + T_l < t \leq (16k+16)T_s + T_l \\ 0 & \text{otherwise} \end{cases} \tag{7}$$

for $k = 0, \ldots, 7$. $T_l = 3.5T_s$ is the lag time in the phase response of SOQPSK-TG, which is fixed and known to the receiver. In the rest of our discussion, we assume the channel observation starts at $t = T_l$, and hence, we ignore T_l. The careful reader may notice that the phase response of Fig. 3 has in fact three parts while (7) expresses it as two segments. This is another approximation we have made in which the phase response during the transition points, which correspond to zero symbols in $\boldsymbol{\alpha}^*$, are approximated by the same function as their subsequent part, i.e. the linear parts. This assumption simplifies our derivations in the following discussion. We do not expect a noticeable loss in the performance of the proposed estimator as each of these transition intervals last only for one symbol time, which is much smaller than the sequence

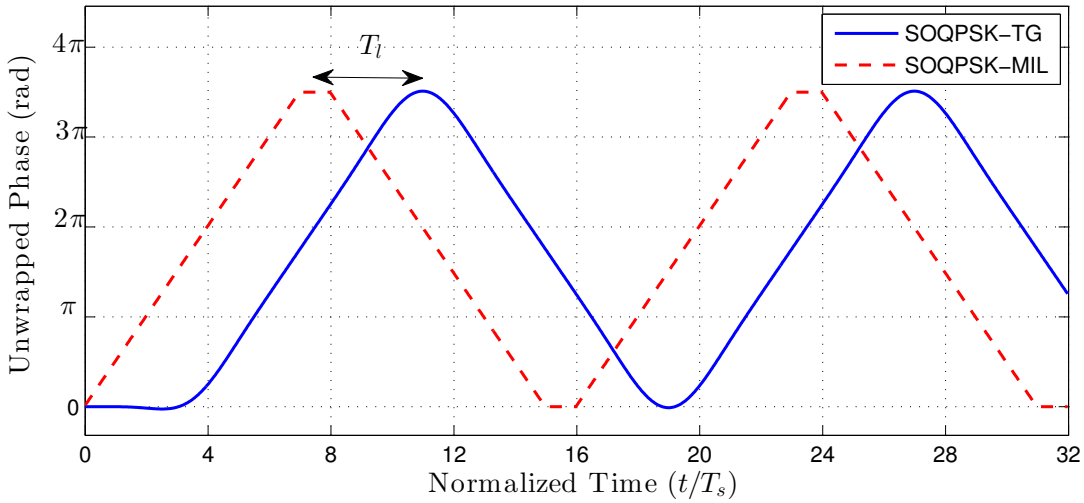

Figure 3: The unwrapped phase response of SOQPSK-MIL and SOQPSK-TG schemes for the first 32 symbols of the iNET preamble.

duration. Our simulation results in Section V confirm this prediction. Thus, we can use (7) to express the baseband SOQPSK-TG signal $s(t)$ during the training sequence transmission as

$$s(t) \approx \begin{cases} \exp[+j\frac{\pi t}{2T_s}] & 16kT_s < t \leq (16k+8)T_s \\ \exp[-j(\frac{\pi t}{2T_s} + \frac{\pi}{2})] & (16k+8)T_s < t \leq (16k+16)T_s \end{cases} \tag{8}$$

We take advantage of the above approximation in order to simplify the LLF and its maximization algorithm. Using (8) in (6) results in a simplified form for the LLF when $\boldsymbol{\alpha}^*$ is transmitted, i.e.

$$\begin{aligned} \Lambda^*(\tilde{f}_d, \tilde{\theta}, \tilde{\tau}) \approx \mathrm{Re}\Big\{ e^{-j\tilde{\theta}} \sum_{k=0}^{7} \Big[& \int_{16kT_s}^{(16k+8)T_s} e^{-j2\pi f_d t} r(t) e^{-j\pi(t-\tau)/2T_s} dt \\ & + \int_{(16k+8)T_s}^{(16k+16)T_s} e^{-j2\pi f_d t} r(t) e^{j\pi(t-\tau)/2T_s} e^{j\pi/2} dt \Big] \Big\} \end{aligned} \tag{9}$$

where $\Lambda^*(\cdot)$ represents the joint LLF given $\boldsymbol{\alpha}^*$. It is evident from (9) that the symbol timing is now decoupled from the frequency offset and can be moved outside the integrals of the LLF. Hence, the joint LLF can be summarized as

$$\Lambda^*(\tilde{f}_d, \tilde{\theta}, \tilde{\tau}) \approx \mathrm{Re}\Big\{ e^{-j\tilde{\theta}} \big[e^{j\pi\tilde{\tau}/2T_s} \lambda_1(\tilde{f}_d) + e^{-j\pi\tilde{\tau}/2T_s} \lambda_2(\tilde{f}_d) \big] \Big\} \tag{10}$$

where

$$\lambda_1(\tilde{f}_d) = \sum_{k=0}^{7} \int_{16kT_s}^{(16k+8)T_s} e^{-j2\pi f_d t} r(t) e^{-j\pi t/2T_s} \, dt \tag{11}$$

and

$$\lambda_2(\tilde{f}_d) = e^{j\pi/2} \sum_{k=0}^{7} \int_{(16k+8)T_s}^{(16k+16)T_s} e^{-j2\pi f_d t} r(t) e^{j\pi t/2T_s} \, dt. \tag{12}$$

Because the estimation parameters are now decoupled, the maximization of the LLF becomes straightforward. Based on (10), we define the normalized symbol timing with respect to the symbol duration as $\varepsilon = \tau/T_s$, which is used in the rest of our discussion. Let us proceed by denoting the term in (10) that corresponds to symbol timing and frequency offset as

$$\Gamma(\tilde{f}_d, \tilde{\varepsilon}) = e^{j(\pi/2)\tilde{\varepsilon}}\lambda_1(\tilde{f}_d) + e^{-j(\pi/2)\tilde{\varepsilon}}\lambda_2(\tilde{f}_d). \tag{13}$$

It is observed that for any trial value of $(\tilde{f}_d, \tilde{\varepsilon})$, $\Lambda^*(\cdot)$ is maximized by choosing $\tilde{\theta}$ such that it rotates $\Gamma(\tilde{f}_d, \tilde{\varepsilon})$ towards the real axis, i.e.,

$$\tilde{\theta} = \arg\{\Gamma(\tilde{f}_d, \tilde{\varepsilon})\}. \tag{14}$$

which reduces the LLF to $|\Gamma(\tilde{f}_d, \tilde{\varepsilon})|$. Thus, the ML estimates of $\tilde{f}_d$ and $\tilde{\tau}$ are found by maximizing

$$|\Gamma(\tilde{f}_d, \tilde{\varepsilon})|^2 = |\lambda_1(\tilde{f}_d)|^2 + |\lambda_2(\tilde{f}_d)|^2 + 2\mathrm{Re}\Big[e^{-j\pi\tilde{\varepsilon}}\lambda_1^*(\tilde{f}_d)\lambda_2(\tilde{f}_d)\Big] \tag{15}$$

with respect to $(\tilde{f}_d, \tilde{\varepsilon})$. The first two terms on the right-hand side of (15) do not depend on $\tilde{\varepsilon}$. Using a similar argument as $\tilde{\theta}$, the third term is maximized by selecting $\tilde{\varepsilon}$ according to

$$\tilde{\varepsilon} = \frac{\arg\{\lambda_1^*(\tilde{f}_d)\lambda_2(\tilde{f}_d)\}}{\pi} \tag{16}$$

such that the term inside the real part operator of (15) becomes purely real and equal to $|\lambda_1(\tilde{f}_d)\lambda_2^*(\tilde{f}_d)|$. Therefore, the maximization of the LLF is now a one dimensional problem that results in the ML estimate of frequency offset, i.e. $\hat{f}_d$. This can be expressed mathematically in the form of

$$\hat{f}_d = \underset{\tilde{f}_d}{\mathrm{argmax}} \Big\{ X(\tilde{f}_d) = |\lambda_1(\tilde{f}_d)| + |\lambda_2(\tilde{f}_d)| \Big\} \tag{17}$$

which leads to the ML estimates of the normalized symbol timing $\hat{\varepsilon}$ and phase offset $\hat{\theta}$ via

$$\hat{\varepsilon} = \frac{\arg\{\lambda_1^*(\hat{f}_d)\lambda_2(\hat{f}_d)\}}{\pi} \tag{18}$$

and

$$\hat{\theta} = \arg\Big\{ e^{j(\pi/2)\hat{\varepsilon}}\lambda_1(\hat{f}_d) + e^{-j(\pi/2)\hat{\varepsilon}}\lambda_2(\hat{f}_d) \Big\} \tag{19}$$

respectively.

IMPLEMENTATION OF THE ML ESTIMATOR

In the previous section, we observed that the maximization of the joint LLF was simplified to computing the maximum of a one-dimensional function with respect to the frequency as defined in (17). Unfortunately, its global maximum cannot be obtained analytically because of the presence of several local maxima. In fact, $\lambda_1(f_d)$ and $\lambda_2(f_d)$ are the form of Fourier transforms of $r(t)$ and should be expected to have fluctuations due to the presence of noise, which results in local maxima. Thus, a grid search is inevitable in order to find the correct frequency offset with confidence. After finding the frequency offset, the other synchronization parameters are easily computed.

According to (11) and (12), each of $\lambda_1(f_d)$ and $\lambda_2(f_d)$ requires computation of 8 integrals with different limits. In order to make them consistent, we define two new signals, i.e. $r_1(t)$ and $r_2(t)$ such that

$$r_1(t) = \begin{cases} r(t) & 16kT_s < t \leq (16k+8)T_s \\ 0 & \text{otherwise} \end{cases} \tag{20}$$

and

$$r_2(t) = \begin{cases} e^{j\pi/2} r(t) & (16k+8)T_s < t \leq (16k+16)T_s \\ 0 & \text{otherwise.} \end{cases} \tag{21}$$

for $0 \leq k \leq 7$. The above modifications to $r(t)$ lead to similar forms for $\lambda_1(f_d)$ and $\lambda_2(f_d)$, where each one requires computation of one integral with a duration of $[0, T_0]$.

So far, we have considered continuous-time functions and integrals in our discussion. However, the received signal must be sampled in practice where the integrals are substituted with summations. We assume that the received signal is sampled N times per symbol resulting in a sampled form of $r[n] = r(nT_s/N)$. Furthermore, we normalize the frequency offset with respect to the sampling frequency, i.e. $\nu = f_d T_s/N$. Therefore, the discrete-time versions of (11) and (12) can be written as,

$$\lambda_1(\tilde{\nu}) = \sum_{n=0}^{NL_0-1} r_1[n] e^{-j\frac{\pi n}{2N}} e^{-j2\pi n\tilde{\nu}} \tag{22}$$

and

$$\lambda_2(\tilde{\nu}) = \sum_{n=0}^{NL_0-1} r_2[n] e^{j\frac{\pi n}{2N}} e^{-j2\pi n\tilde{\nu}} \tag{23}$$

respectively where $r_1[n]$ and $r_2[n]$ are sampled versions of $r_1(t)$ and $r_2(t)$ at $t = nT_s/N$ respectively. Finally, f_d should be replaced by ν in (17) in order to estimate the normalized frequency offset.

The computation of (22) and (23) for different trial values of ν resembles the discrete Fourier transform (DFT) operation where $\tilde{\nu}$ is replaced by trial discrete frequencies. These operations can be performed efficiently using fast Fourier transform (FFT) algorithms. The number of these trial frequencies is the same as the length of the above summations, i.e. NL_0. Therefore, the frequency estimate requires two FFT operations each of which has a length equal to the total number of samples collected from the preamble. Prior to the computation of the FFTs, $r_1[n]$ and $r_2[n]$ have to be rotated by $\exp(j\frac{\pi n}{2N})$ and $\exp(-j\frac{\pi n}{2N})$ respectively, which becomes trivial for $N = 1$. The FFT operations generate trial values of $\lambda_1(\tilde{\nu})$ and $\lambda_2(\tilde{\nu})$ such that $\tilde{\nu} \in \{0, 1/NL_0, \ldots, (NL_0-1)/NL_0\}$. The $\tilde{\nu}$ which maximizes (17) is chosen as the estimated normalized frequency offset.

Due to the discrete nature of the FFT, the frequency estimation performance is limited by the resolution of the FFTs, i.e. the distance between the discrete frequency components. In (22) and (23), this resolution is $1/NL_0$, which can be viewed as $1/L_0$ with respect to the symbol rate, i.e. $1/T_s$. This limits the accuracy of frequency offset estimation for short and moderate length preambles. Additionally, a low frequency resolution may have a ripple effect on the accuracy of symbol timing and phase estimates. In order to improve the accuracy of the frequency estimation, two approaches are considered. The first approach is to zero pad the FFT operands in (22) and (23) such that both FFTs have an increased size of $N_f = K_f NL_0$. Here, we assume that the original FFT size and K_f are powers of two. This procedure results in a frequency resolution of $1/K_f L_0$ with respect to the symbol rate. The second method to tackle

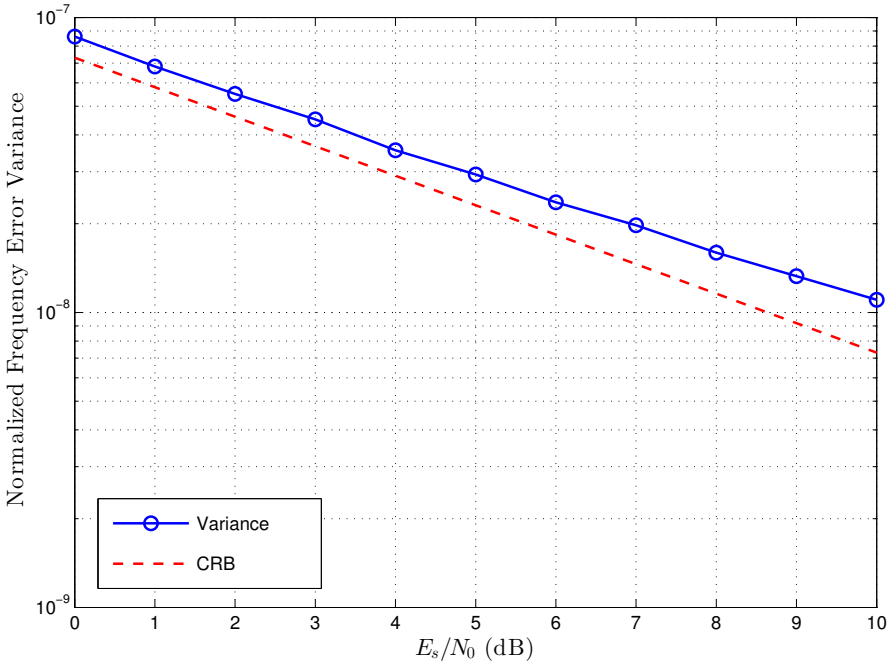

Figure 4: The variance of frequency offset estimation for SOQPSK-TG when $L_0 = 128$. The frequency is normalized with respect to the symbol rate.

this issue is by employing an interpolator such that the actual location of maximizing frequency–between two adjacent discrete frequencies–is estimated. Here, we resort to a Gaussian interpolator [4] that can be expressed as

$$\hat{\nu} = \hat{\nu}_0 + \frac{1}{2K_f N L_0} \frac{\log X(\hat{\nu}_{-1}) - \log X(\hat{\nu}_1)}{\log X(\hat{\nu}_{-1}) + \log X(\hat{\nu}_1) - 2\log X(\hat{\nu}_0)} \tag{24}$$

where $\hat{\nu_0}$ represents the maximizing frequency resulting from (17). $\hat{\nu}_{-1}$ and $\hat{\nu}_1$ denote the discrete frequency components immediately before and after $\hat{\nu_0}$ respectively in terms of the FFT operation.

Once the final frequency offset estimate is available through the above interpolation, it is inserted in (22) and (23) to calculate $\lambda_1(\hat{\nu})$ and $\lambda_2(\hat{\nu})$ respectively. This process improves the precision of these variables, which were originally generated from the FFTs, by taking into account the effect of the interpolation. Finally, they are used in (18) to compute symbol timing $\hat{\varepsilon}$, and then, in (19) to estimate the carrier phase $\hat{\theta}$.

SIMULATION RESULTS

The estimation error variances corresponding to the normalized frequency offset, normalized symbol timing and carrier phase are depicted in Figs. 4, 5 and 6 respectively for SOQSPK-TG. In all plots, the preamble of Fig. 2 is employed when $L_0 = 128$ and $N = 2$. Moreover, we have considered $K_f = 2$ along with the Gaussian interpolator of (24). The estimation error variances are calculated via simulations. Additionally, we have included the CRB plots given in [5], which are lower bounds on the estimation error variance of their corresponding parameter. Fig. 4 shows that the frequency estimator performs only

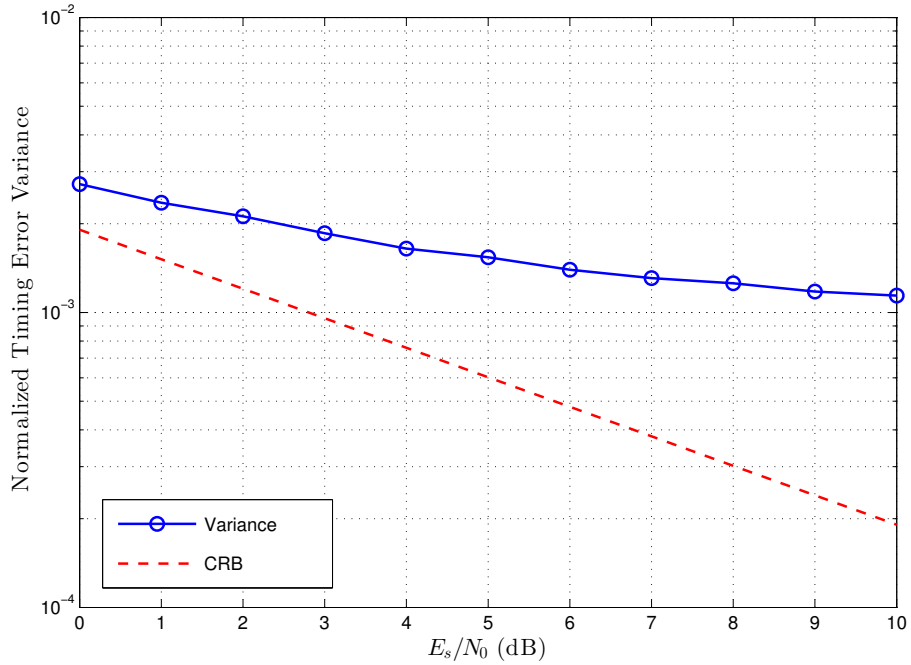

Figure 5: The variance of symbol timing estimation for SOQPSK-TG when $L_0 = 128$. The symbol timing is normalized with respect to the symbol duration.

about 1 dB away from the CRB for low to moderate E_s/N_0 values. The normalized symbol timing error variance is depicted in Fig. 5 in which the performance degrades at high SNRs. Our investigations show that the symbol timing estimation error increases as τ becomes larger, which in turn increases the errors in computation of the LLF due to our approximations. The main source of these errors is the approximation in (6) where we have assumed $\hat{\tau} = 0$ in the integral limits. Nevertheless, the estimation precision is still adequate for reliable demodulation especially at low SNRs. In fact, CPM signals (including SOQPSK) are quite tolerant of symbol timing errors compared to phase errors [6]. Finally, the phase error variance is plotted in Fig. 6, which indicates that the performance of our proposed algorithm is less than 1 dB away from the theoretical limit at low SNRs where the synchronization is at its hardest. Unlike symbol timing estimation, the errors in phase estimation are mainly caused by frequency estimation errors, which can be improved by using a larger FFT.

CONCLUSION

We presented a DA ML algorithm for synchronization of SOQPSK-TG signals in burst-mode transmissions for aeronautical telemetry. The proposed algorithm is designed according to the specific pattern of the preamble sequence intended for the iNET. It first estimates the frequency offset from the received preamble using FFT and interpolation operations. Once the frequency offset is estimated, the symbol timing and carrier phase are subsequently estimated via simple closed-form expressions. The performance of the proposed algorithm was examined using simulations. It was shown that our method performs within 1 dB of the theoretical CRB at low to moderate SNRs for frequency and phase estimations. It also estimates the symbol timing with sufficient precision especially at low SNRs.

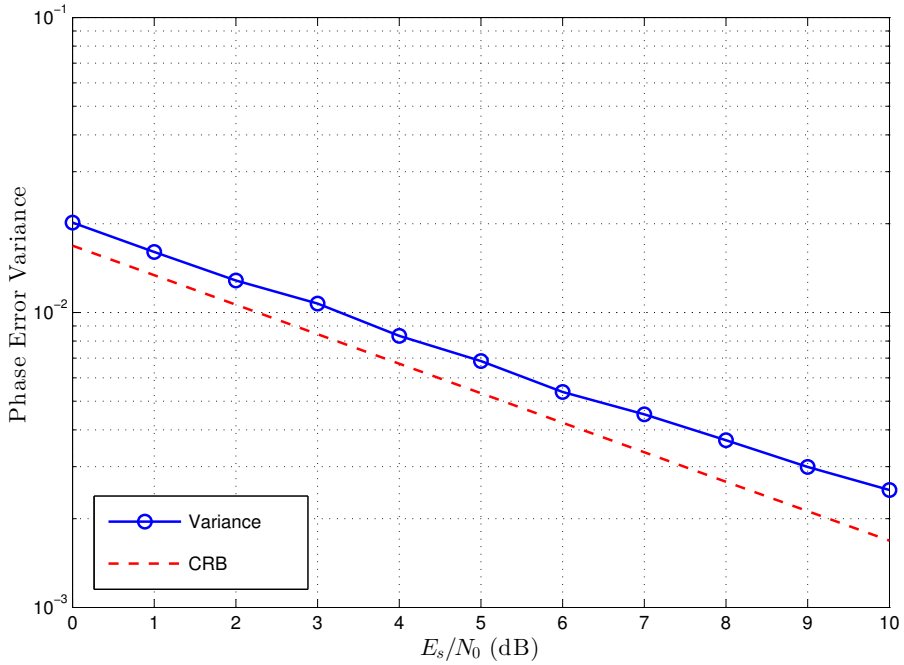

Figure 6: The variance of carrier phase estimation for SOQPSK-TG when $L_0 = 128$.

ACKNOWLEDGEMENT

The authors would like to thank the Test Resource Management Center (TRMC) Test and Evaluation/Science and Technology (T&E/S&T) Program for their support. This work was funded by the T&E/S&T Program through the U.S. Army Program Executive Office for Simulation, Training and Instrumentation (PEO STRI), contract number W900KK-11-C-0032 for Burst Mode Synchronization for SOQPSK (SYNC). The release number for this publication is 412TW-PA-13278.

REFERENCES

[1] M. J. Dapper and T. J. Hill, "SBPSK: a robust bandwidth-efficient modulation for hard-limited channels," in *IEEE Military Communications Conference 1984*, (Los Angeles, CA), pp. 458–463, 1984.

[2] Range Commanders Council Telemetry Group, Range Commanders Council, White Sands Missile Range, New Mexico, *IRIG Standard 106-04: Telemetry Standards*, 2004. [Online] (Available: http://www.ntia.doc.gov/osmhome/106.pdf).

[3] M. Morelli, U. Mengali, and G. Vitetta, "Joint phase and timing recovery with CPM signals," *IEEE Transactions on Communications*, vol. 45, pp. 867–876, July 1997.

[4] M. Gasior and J. L. Gonzalez, "Improving FFT frequency measurement resolution by parabolic and Gaussian spectrum interpolation," in *AIP Conf. Proc.*, vol. 732, (Knoxville, TN), pp. 276–285, AIP, 2004.

[5] E. Hosseini and E. Perrins, "The Cramér-Rao bound for training sequence design for burst-mode CPM," *IEEE Trans. Commun.*, vol. 61, pp. 1–12, Jun. 2013.

[6] U. Mengali and A. N. D'Andrea, *Synchronization Techniques for Digital Receivers*. Plenum Press, 1997.